

- [6] J. Baena, L. Jelinek, and R. Marqués, "Towards a systematic design of isotropic bulk magnetic metamaterials using the cubic point groups of symmetry," *Phys. Rev. B*, vol. 76, no. 24, p. 245115, 2007.
- [7] V. A. Fedotov, P. L. Mladyonov, S. L. Prosvirnin, and N. I. Zheludev, "Planar electromagnetic metamaterial with a fish scale structure," *Phys. Rev. E*, vol. 72, p. 056613, 2005.
- [8] M. N. Kawakatsu, V. A. Dmitriev, and S. L. Prosvirnin, "Microwave frequency selective surfaces with high Q-factor resonance and polarization insensitivity," *J. Electromagn. Waves Appl.*, vol. 24, pp. 261–270, 2010.
- [9] V. A. Fedotov, A. V. Rogacheva, N. I. Zheludev, P. L. Mladyonov, and S. L. Prosvirnin, "Mirror that does not change the phase of reflected waves," *Appl. Phys. Lett.*, vol. 88, p. 091119, 2006.
- [10] G. W. Hanson, "Dyadic Green's functions for an anisotropic, non-local model of biased graphene," *IEEE Trans. Antennas Propag.*, vol. 56, no. 3, pp. 747–757, Mar. 2008.
- [11] E. Carrasco, M. Tamagnone, J. R. Mosig, T. Low, and J. Perruisseau-Carrier, "Gate-controlled mid-infrared light bending with aperiodic graphene nanoribbons array," *Nanotechnology*, vol. 26, no. 3, p. 134002, 2015.

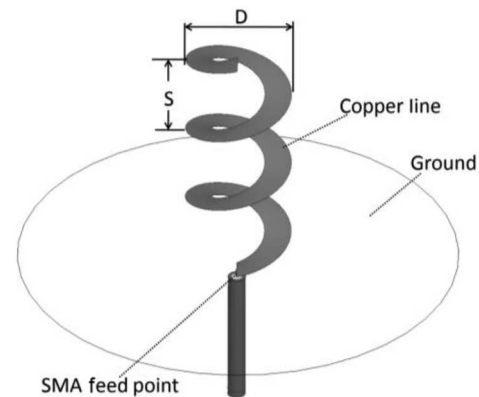


Fig. 1. Geometry of standard helical antenna.

TABLE I  
OPTIMAL PARAMETERS OF STANDARD HELICAL ANTENNA

Parameter	Optimum range
Circumference	$3\lambda/4 < C < 4\lambda/3$
Pitch Angle	$12^\circ < \alpha < 14^\circ$
Number of Turns	$3 < N$
Ground Plane Diameter	At least $0.5\lambda$

## An Origami Reconfigurable Axial-Mode Bifilar Helical Antenna

Xueli Liu, Shun Yao, Benjamin S. Cook, Manos M. Tentzeris, and Stavros V. Georgakopoulos

**Abstract**—This communication presents a new reconfigurable origami bifilar helical antenna. This antenna can change its operating frequencies by changing its height. Also, analytical equations for the design of such antennas are derived based on an equivalent model of a standard helical antenna. An origami bifilar helical antenna is designed and its performance is verified using simulations and measurements.

**Index Terms**—Axial mode, helical antenna, origami antenna.

### I. INTRODUCTION

Origami, which means “paper folding” in Japanese, has been used in a wide range of applications, such as, medical devices, spaceborne systems, and energy harvesting [1]. Limited previous work has been performed on origami electromagnetic structures [1]–[8]. Origami electromagnetic geometries have significant advantages for structures that need to fold in order to miniaturize their size, and unfold in order to operate [9], [10].

Axial-mode helical antennas are very suitable for spaceborne and airborne communications [11]. Reconfigurable helical antennas based

Manuscript received January 29, 2015; revised September 19, 2015; accepted September 20, 2015. Date of publication September 24, 2015; date of current version November 25, 2015. This work was supported by the National Science Foundation under Grant EFRI 1332348.

X. Liu, S. Yao, and S. V. Georgakopoulos are with the Department of Electrical and Computer Engineering, Florida International University, Miami, FL 33174 USA (e-mail: xliu038@fiu.edu; syao002@fiu.edu; georgako@fiu.edu).

B. S. Cook is with Kilby Labs, Texas Instruments, Dallas, TX 75243 USA (e-mail: bcook40@mail.gatech.edu).

M. M. Tentzeris is with the School of Electrical and Computer Engineering, Georgia Institute of Technology, Atlanta, GA 30332 USA (e-mail: tentze@ece.gatech.edu).

Color versions of one or more of the figures in this communication are available online at <http://ieeexplore.ieee.org>.

Digital Object Identifier 10.1109/TAP.2015.2481922

on shape memory alloy have also been developed [12], [13]. In this communication, an origami reconfigurable axial-mode helical antenna is presented, which is also very well suited for spaceborne and airborne applications not only due to its electromagnetic performance but also due to its compatibility and deployability.

First, an analytical method for designing origami helical antennas is presented in Section II. Design formulas for origami helical antennas, which are equivalent to the design empirical formulas of standard helical antennas, are derived. Second, a reconfigurable origami bifilar antenna is designed and its performance is validated using simulations and measurements in Section III. The proposed antenna is constructed on paper substrate thereby providing a light-weight, low-cost, multifunctional, compact, and possibly disposable design.

### II. ANALYSIS OF AXIAL-MODE ORIGAMI HELICAL ANTENNA

#### A. Standard Axial Mode Helical Antenna

Helical antennas have two principle modes: the normal (broadside) and the axial (end-fire) mode. However, the axial mode is more practical of operation as it has only one major lobe radiating along the axis of the helix [14]. The empirical optimum parameters for a standard axial-mode circularly polarized helical antenna, which is shown in Fig. 1, are given in Table I; where,  $S$  is the pitch between two adjacent turns and  $C = \pi D$  is the circumference of the helix [14], [15]. Also, the pitch angle  $\alpha$  and the total length of copper line  $L$  are given by [14]

$$\tan \alpha = S/C \quad (1)$$

$$L = N \cdot (S^2 + C^2)^{1/2}. \quad (2)$$

#### B. Analysis of Origami Helical Model

In this section, an analytical method will be developed for designing an origami helical antenna that mimics a standard helical antenna with specific parameters  $D$ ,  $\alpha$ , and  $N$ .

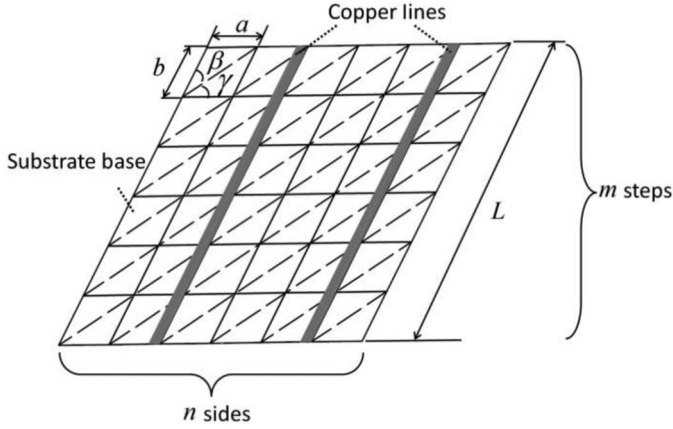


Fig. 2. Folding pattern of origami helix.

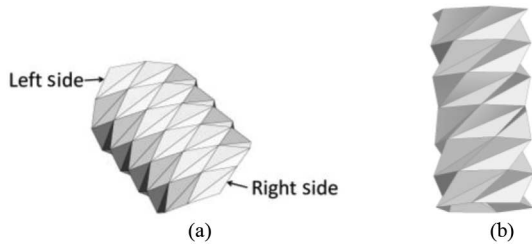


Fig. 3. Procedure of folding the origami cylinder substrate base. (a) Form valleys and hills. (b) Form the origami cylinder by connecting the left side to the right side.

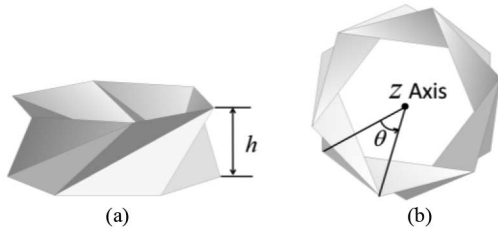


Fig. 4. Geometry of each step of the origami cylinder substrate base. (a) Perspective view. (b) Top view.

The folding pattern [16], which is used to fold the origami cylinder base of the helix, is shown in Fig. 2. The solid lines are hills and dashed lines are valleys. The conductive (i.e., copper) lines are placed along sides  $b$ , as illustrated in Fig. 2. The total length of each conductive arm is  $L$ .

The origami cylinder base of the helical antenna, as shown in Fig. 3(b), is obtained by first folding the pattern of Fig. 2 to obtain the geometry of Fig. 3(a), and then connecting the left side of Fig. 3(a) to its right side from top to the bottom [4]. The height of each step of the origami cylinder is defined as  $H$  and the angle between each step and its adjacent step is defined as  $\theta$ , as shown in Fig. 4.

The relationships between all the geometric parameters of the origami helical antenna are listed in Table II, where *ratio* is the aspect ratio of each parallelogram unit of the pattern in Fig. 2, and  $m$  is the total number of steps. Also, the number of sides  $n$ , and *ratio* should meet the following conditions so that the pattern of the origami helix is foldable

$$n \geq 4, \quad n \in N^+ \quad (3)$$

$$0 < \text{ratio} < n/4. \quad (4)$$

TABLE II  
GEOMETRIC PARAMETERS OF ORIGAMI HELICAL ANTENNAS

Parameters of original helix	Relationships among parameters
$m, n, a, b, \text{ratio}, \beta, \gamma, L, h, \theta$	$\text{ratio} = b/a$
	$\beta = 180^\circ/n$ [9]
	$\gamma = \sin^{-1} \left[ \text{ratio} \cdot \sin \left( \frac{180^\circ}{n} \right) \right]$
	$L = m \cdot b = m \cdot a \cdot \text{ratio}, m \in N^+$
	$h = \sqrt{b^2 - \frac{a^2 \cdot \sin^2 \left( \frac{\theta}{2} \right)}{\sin^2 \left( \frac{180^\circ}{n} \right)}}$

TABLE III  
RELATIONSHIPS BETWEEN STANDARD AND ORIGAMI HELICES

Standard helix	Relationships	Equivalent origami helix
$D, \alpha, N$	$a = \pi D/n$ $\theta = 2 \arcsin \left[ N \cdot \frac{n}{m} \cdot \sin \left( \frac{180^\circ}{n} \right) \right]$ $\text{ratio} = \sec \alpha \cdot \sin \left( \frac{\theta}{2} \right) / \sin \left( \frac{180^\circ}{n} \right)$	$m$ (given), $n$ (given), $a, \text{ratio}, \theta$
Origami helix	Relationships	Equivalent origami helix
$m, n, a, b, \theta$	$S = nah / \sqrt{b^2 - h^2}$ $\tan \alpha = \sqrt{\frac{(b/a)^2 \cdot \sin^2 \left( \frac{180^\circ}{n} \right)}{\sin^2 \left( \frac{\theta}{2} \right)} - 1}$ $N = m \cdot \sin \left( \frac{\theta}{2} \right) / \left[ n \cdot \sin \left( \frac{180^\circ}{n} \right) \right]$	$S, \alpha, N$

With any given standard helical antenna, its equivalent origami helical antenna could be derived when  $m$  and  $n$  are specified, and vice versa, as listed in Table III. Specifically, the standard helix and origami helix are equivalent in terms of the values of pitch  $S$ , pitch angle  $\alpha$ , number of turns  $N$ , and total length  $L$ . Also, the circumference of the standard helix is equal to the perimeter of the origami helix.

The empirical maximum gain of a numerically modeled standard helix can be expressed as [14]

$$G_{\max}(\text{dB}) = 10.25 + 1.22L/\lambda - 0.0726(L/\lambda)^2. \quad (5)$$

Also, the analytical maximum gain of an origami helix, which satisfies the conditions of Table I, can be expressed as

$$G_{\max}(\text{dB}) = 10.25 + 1.22 \frac{m}{n} \cdot \text{ratio} - 0.0726 \left( \frac{m}{n} \cdot \text{ratio} \right)^2. \quad (6)$$

### C. Comparison of Standard Helical Antennas With Equivalent Origami Helical Antennas

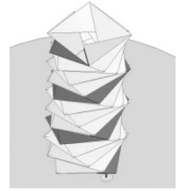
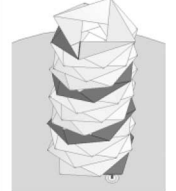
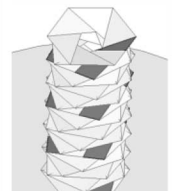
An axial-mode standard helical monofilar antenna is designed and its parameters are described in Table IV. The parameters of the equivalent origami helical monofilar antennas are calculated with different values of  $n$  or  $m$ , and are shown in Table V.

The simulated  $S_{11}$  of both the standard helical antenna and the equivalent origami helical antennas is shown in Fig. 5. The offset distance between these antennas and their corresponding ground planes

TABLE IV  
 GEOMETRIC PARAMETERS OF THE STANDARD HELICAL ANTENNA

$D$	$S$	$\tan\alpha$	$N$
48 mm	37 mm	0.245	3

 TABLE V  
 CALCULATED PARAMETERS OF EQUIVALENT ORIGAMI HELICAL ANTENNAS WITH DIFFERENT FOLDING PATTERNS

	$m = 13$	$m = 15$	$m = 18$
$n = 4$	$a = 37.7$ mm ratio = 0.95 $\theta = 81.5^\circ$	$a = 37.7$ mm ratio = 0.82 $\theta = 68.9^\circ$	$a = 37.7$ mm ratio = 0.69 $\theta = 56.3^\circ$
			
	$n = 4$	$n = 5$	$n = 6$
$m = 13$	$a = 37.7$ mm ratio = 0.95 $\theta = 81.5^\circ$	$a = 30.2$ mm ratio = 1.19 $\theta = 85.4^\circ$	$a = 25.1$ mm ratio = 1.43 $\theta = 87.6^\circ$
			

is 3.5 mm. The radius of the circular ground planes is 100 mm, and the widths and thicknesses of the copper traces are 12 and 0.1 mm, respectively, for all the models, which are excited with a 50- $\Omega$  SMA connector. All simulations are performed using ANSYS HFSS. The simulated performances between the proposed standard helical antenna and its equivalent origami helical antennas are listed in Table VI. During the 3-dB gain bandwidths, the side lobe stays 10-dB lower than the main lobe for all the antennas.

The following conclusions can be drawn from Table VI.

- 1) The equivalent origami helical antennas can operate as well as the standard helical antenna in terms of maximum gain ( $< 1$ -dB difference) and 3-dB gain bandwidth ( $\pm 2.6\%$  difference).
- 2) The RHCP bandwidth of the standard antenna is 5.1%–10.8% larger than that of the equivalent origami antennas.
- 3) A different  $m$  or  $n$  in the origami pattern will change the geometry of the origami antenna, and a larger  $n$  improves the CP bandwidth.

Based on Table II, reconfigurable origami helical antennas that can operate at various frequencies of interest can be parametrically modeled and designed. As an example, a bifilar reconfigurable origami helical antenna is introduced in Section III. Furthermore, the proposed origami helical antennas can be folded to fit in compact storage/launching compartments thereby providing significant savings of volume for spaceborne and airborne applications such as satellites. Specifically, when the proposed origami structure totally collapses it occupies its minimum volume of  $\frac{mntn^2a^2}{2\pi}$ , and when it fully deploys it occupies its maximum volume of  $\frac{mb \sin(\beta+\gamma)n^2a^2}{4\pi}$ , where  $t$  is the thickness of the origami substrate base. In order to quantify the volume

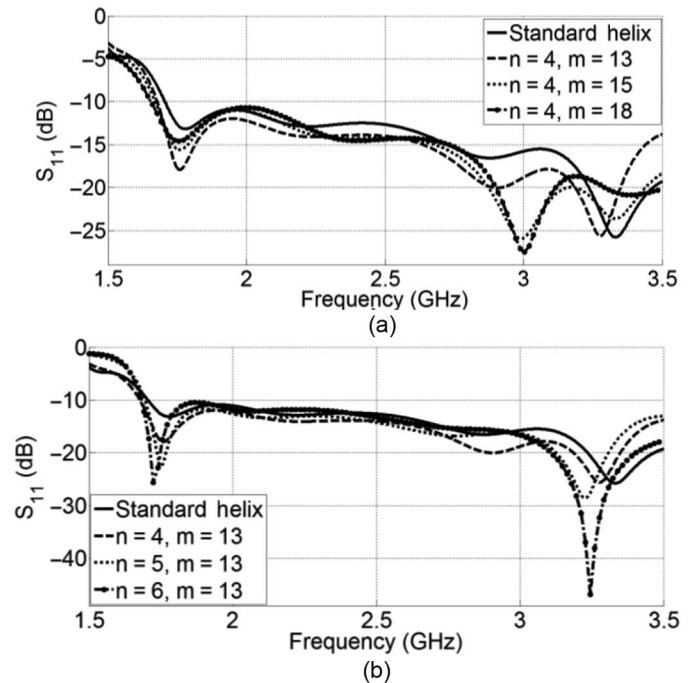


Fig. 5. Comparison of  $S_{11}$  of a standard helical antenna and its equivalent origami helical antennas. (a) Equivalent origami helix with  $n = 4$ ,  $m = 13, 15, 18$ . (b) Equivalent origami helix with  $m = 13$ ,  $n = 4, 5, 6$ .

 TABLE VI  
 PERFORMANCE COMPARISON OF STANDARD HELICAL MONOFILAR ANTENNA AND ITS EQUIVALENT ORIGAMI HELICAL MONOFILAR ANTENNAS

Performance		3-dB gain bandwidth (GHz)	RHCP bandwidth (axial ratio < 3 dB) (GHz)	Maximum realized gain (dB)
Antennas				
Standard helix		1.75–3.3 (1.89:1)	1.78–3.3 (1.85:1)	12.87
Origami $n = 4$	$m = 13$	1.65–3.15 (1.91:1)	1.89–3.15 (1.67:1)	12.23
	$m = 15$	1.7–3.2 (1.88:1)	1.87–3.2 (1.71:1)	12.29
	$m = 18$	1.65–3.1 (1.88:1)	1.81–3.1 (1.71:1)	12.28
Origami $m = 13$	$n = 4$	1.65–3.15 (1.9:1)	1.89–3.15 (1.67:1)	12.23
	$n = 5$	1.7–3.25 (1.91:1)	1.88–3.25 (1.73:1)	11.94
	$n = 6$	1.7–3.3 (1.94:1)	1.88–3.3 (1.76:1)	12.08

savings that this origami structure provides during its storage, the compactness factor is defined as

$$F_{compact} = \frac{Volume_{max}}{Volume_{min}} = \frac{b \sin(\beta + \gamma)}{2t}. \quad (7)$$

### III. RECONFIGURABLE ORIGAMI BIFILAR HELICAL ANTENNA

The empirical frequency range of operation of the origami helical antenna can be written as

$$\frac{3c}{4na} < f < \frac{4c}{3na}. \quad (8)$$

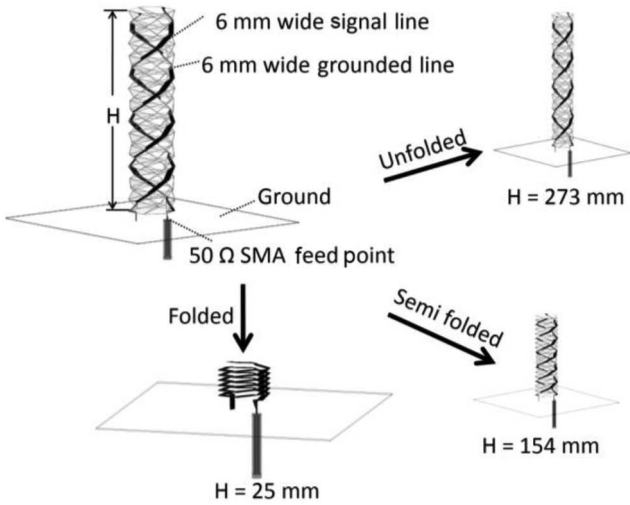


Fig. 6. Origami bifilar helical antenna model at different states of H.

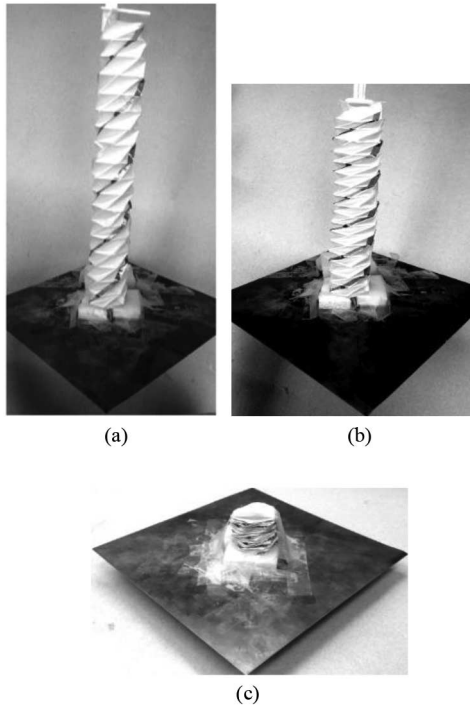


Fig. 7. Prototype of reconfigurable origami bifilar helical antenna with different heights H. (a) H = 273 mm. (b) H = 154 mm. (c) H = 25 mm.

Also, the proposed origami helical antenna can be designed to exhibit frequency reconfigurability by changing  $\theta$  or  $h$  (which in turn changes the pitch angle  $\alpha$ ) and achieve optimal gain at multiple frequencies in the frequency range of (8).

Here, an origami bifilar antenna is designed, as shown in Fig. 6. One helix is connected to the signal excitation (center conductor of SMA) and the second helix is grounded.

The number of steps  $m = 18$ , the number of sides  $n = 6$ , the side length of each element in the pattern  $a = 22.5$  mm, and the  $ratio = 1$ . The height of the antenna can vary as the origami structure can collapse and expand. The total height of this antenna is  $H = m \cdot h$ . A square ground plane is used with a side length of 200 mm. The distance between the antenna and the ground is 13.7 mm, which was determined by the thickness of the polyethylene foam (with  $\epsilon_r = 1.2$ )

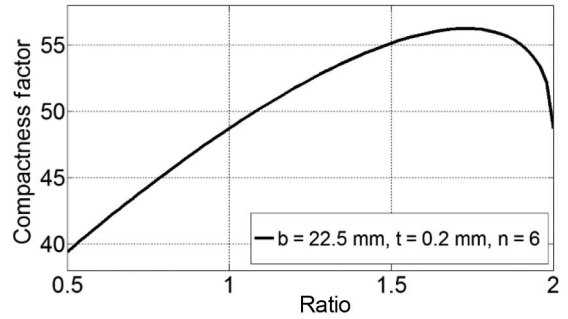


Fig. 8. Compactness factor versus ratio with fixed  $b$ ,  $t$ , and  $n$ .

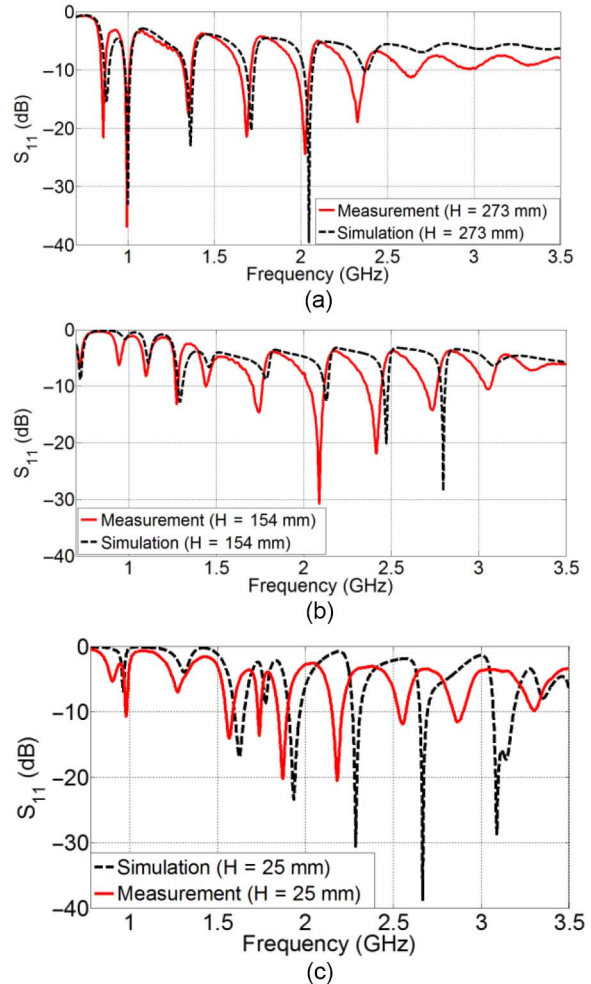


Fig. 9. Return loss of origami bifilar helix for different antenna heights H. (a) H = 273 mm. (b) H = 154 mm. (c) H = 25 mm.

base that was used to support the antenna and prevent it from being shorted. The distance between the grounded line and the signal line is 29 mm. The grounded helix enables the bifilar to radiate at the lowest frequency axially when the antenna is fully deployed (i.e., is at its maximum operating height). The prototype of the origami bifilar is shown in Fig. 7. This antenna was constructed using 0.1-mm-thick copper tape on 0.2-mm-thick sketching-paper substrate without any coating. The copper tape is glued on the paper and creased with the paper, so that it will stay attached to the paper base when the antenna is being folded and unfolded. The paper substrate was modeled in the simulations with a relative permittivity  $\epsilon_r$  of 3.2 [17]. Our simulation results

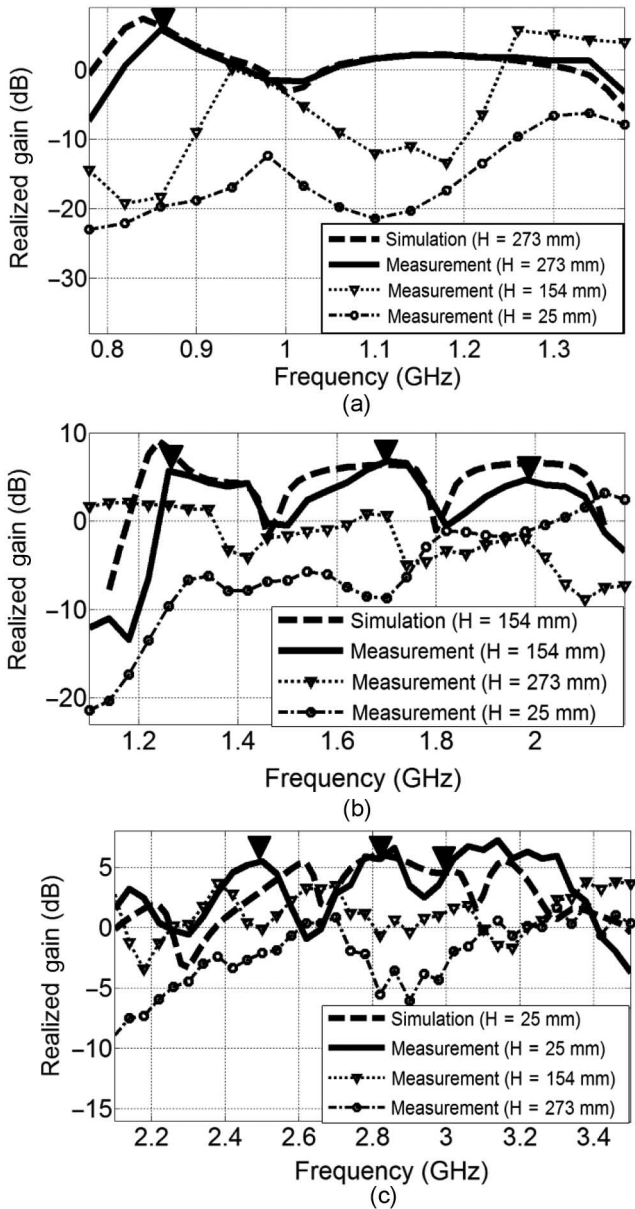


Fig. 10. Realized gain at zenith for three different states. (a) Unfolded state ( $H = 273$  mm). (b) Semifolded state ( $H = 154$  mm). (c) Folded state ( $H = 25$  mm).

show that the dielectric constant of paper does not significantly affect the gain or polarization of the antenna, but it does shift its resonant frequencies compared to the case with no substrate. Also, the copper tape is suitable for repeated folding and unfolding and does not crack. The copper tape has a measured conductivity of  $4.4 \times 10^5$  S/m and does not have a significant effect on the antenna gain. The height  $H$  of the prototype antenna was controlled by applying a force at its top face. Also, the prototype antenna was fixed at different states using 3-D printed supports that were made out of polylactic acid with  $\epsilon_r = 3.25$  [18], which are not included in simulations. The compactness factor of this antenna design as defined by (7) is plotted in Fig. 8 versus the *ratio* for  $b = 22.5$  mm,  $t = 0.2$  mm, and  $n = 6$ . Fig. 8 shows that the theoretically optimum compactness factor of 56.25 is achieved when the *ratio* = 1.73.

The simulated and measured  $S_{11}$  for three different heights  $H$  is illustrated in Fig. 9. The simulated and measured realized gains at

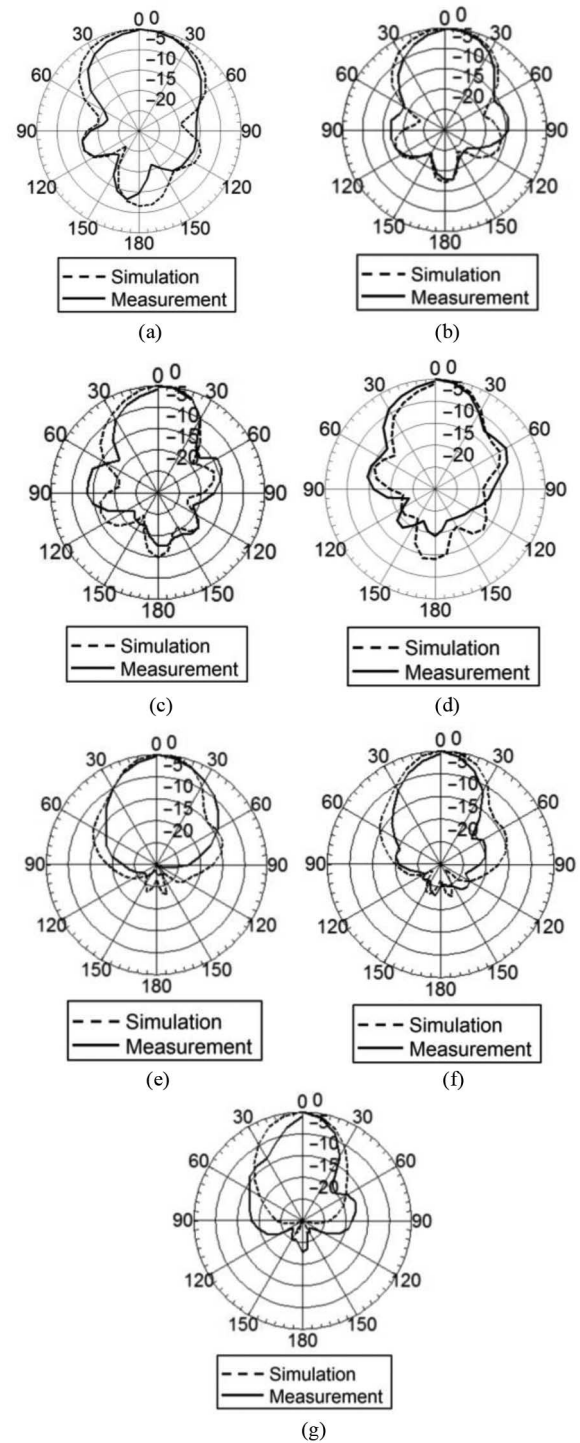


Fig. 11. Normalized elevation patterns of the origami bifilar helical antenna at the operating frequencies of the three states (i.e., heights). (a)  $H = 273$  mm at 0.86 GHz. (b)  $H = 154$  mm at 1.27 GHz. (c)  $H = 154$  mm at 1.7 GHz. (d)  $H = 154$  mm at 1.98 GHz. (e)  $H = 25$  mm at 2.49 GHz. (f)  $H = 25$  mm at 2.81 GHz. (g)  $H = 25$  mm at 3 GHz.

zenith for the unfolded state ( $H = 273$  mm), the semifolded state ( $H = 154$  mm), and the folded state ( $H = 25$  mm) in different operating frequency bands are illustrated in Fig. 10. The measured results show that this bifilar origami helix is a reconfigurable antenna that can operate at different frequencies by changing its height. The operating frequencies of each state are depicted with solid triangles in Fig. 10.

TABLE VII  
MEASURED REALIZED GAIN AT THE OPERATING FREQUENCIES OF THE 3 STATES OF THE ORIGAMI BIFILAR HELIX

Frequency (GHz) \ Antenna height H (mm)	0.86	1.27	1.7	1.98	2.49	2.81	3
273	5.85	1.80	-0.58	-2.06	-2.11	-5.54	-2.00
154	-18.35	6.53	6.79	4.69	-0.13	-0.69	1.62
25	-19.73	-9.63	-8.7	-1.18	5.98	5.81	5.70

TABLE VIII  
MEASURED PERFORMANCES OF THE BIFILAR HELICAL ORIGAMI ANTENNA FOR THREE DIFFERENT HEIGHTS

Antenna height H (mm)	273	154			25		
Operating frequency (GHz)	0.86	1.27	1.7	1.98	2.49	2.81	3
Measured realized gain (dB)	5.85	6.53	6.79	4.69	5.98	5.81	5.7
Measured E-plane BW (°)	82	59	45	44	61	44	41
Measured H-plane BW (°)	75	50	44	40	57	46	40
Measured AR (dB)	7.54	7.64	12.5	7.67	4.77	3.19	3.89
Measured AR without 3-D printed supports (dB)	19.2	0.56	0.24	0.55	5.78	3.21	2.23

It should also be noted that this origami bifilar helical antenna is designed so that it operates in axial mode at all the indicated operating frequencies of the three states (i.e., heights). The slight discrepancy between the simulated and measured gain presented in Fig. 10 can be attributed to the fact that the prototype of the origami antenna was built by hand, thereby not being exactly the same as the simulated one. The largest discrepancy between simulated and measured gain occurs in Fig. 10(c) because for the antenna height of 25 mm, the spacing between each step of the antenna becomes very small; therefore, slight geometrical differences between the simulation model and the prototype are expected to result in larger discrepancies.

Table VIII illustrates the measured performances of the origami antenna for three different antenna heights. It can be seen from Fig. 10 and Table VIII that the 3-D printed supports did not impact much on  $S_{11}$  and realized gain, while the axial ratio (AR) was impacted more by the supports. The volumes occupied by the origami antenna at the unfolded, semifolded, and folded states are 396, 223, and 36 cm<sup>3</sup>, respectively. The normalized elevation-plane patterns are shown in Fig. 11 at the operating frequencies of each state. It is seen that at higher operating frequencies the back lobes become smaller, which is expected since at higher frequencies the ground plane is electrically larger.

Our findings can be summarized as follows.

- 1) The compactness factor of this antenna as defined by (7) is 48.71, and the maximum foldable compactness factor is 55.14 when  $ratio = 1.5$  according to (4), as shown in Fig. 8.

- 2) This antenna exhibits optimum performance only at the following frequencies listed for each height: (a) 0.86 GHz for  $H = 273$  mm, (b) 1.27, 1.7, and 1.98 GHz for  $H = 154$  mm, and (c) 2.49, 2.81, and 3 GHz for  $H = 25$  mm, as shown in Fig. 10.
- 3) Each state exhibits a higher gain at its own operating frequencies than the gains of the other two states at these frequencies, as shown in Fig. 10 and Table VII.
- 4) Measured AR without supports validated that this antenna is circularly polarized (AR < 2 dB) at 1.27, 1.7, and 1.98 GHz when  $H = 154$  mm, as shown in Table VIII.
- 5) Fig. 11 illustrates that our origami bifilar helical antenna operates in axial mode at all the listed operating frequencies above with maximum gain at zenith.

#### IV. CONCLUSION

This communication examines how to design origami axial-mode helical antennas based on an equivalent model of the standard axial-mode helical antenna. It is shown that origami helical antennas are reconfigurable, i.e., they can change their operating frequencies by changing their heights. A reconfigurable axial mode origami bifilar antenna was designed on a paper substrate and its performances were validated through simulations and measurements. This antenna has the potential to be applied in sensing and differentiating signals in multi-bands. Our future research direction would be to develop more robust designs of the antenna with optimum supports and to develop new deploying mechanism so it can withstand the extreme environment to be applied in space communications.

#### REFERENCES

- [1] K. Miura and M. Natori, "2-D array experiment on board a space flyer unit," *Space Solar Power Rev.*, vol. 5, pp. 345–356, 1985.
- [2] G. M. Olson, S. Pellegrino, and J. Costantine, "Structure architectures for a deployable wideband UHF antenna," in *Proc. Amer. Inst. Aeronaut. Astronaut.*, Apr. 2012, pp. 1–10.
- [3] S. Melais, T. M. Weller, C. M. Newton, R. W. Smith, and C. A. Gamlen, "Origami packaging-novel printed antenna technology for ad-hoc sensor applications," in *Proc. 40th Int. Symp. Microelectron.*, 2007, pp. 22–29.
- [4] X. Liu, S. Yao, and S. V. Georgakopoulos, "Reconfigurable spherical helical electrically small antenna in UHF band," in *Proc. Antennas Propag. Soc. Int. Symp. (APSURSI)*, Memphis, TN, USA, 2014, pp. 368–369.
- [5] S. Yao, X. Liu, S. V. Georgakopoulos, and M. M. Tentzeris, "A novel tunable origami accordion antenna," in *Proc. Antennas Propag. Soc. Int. Symp. (APSURSI)*, Memphis, TN, USA, 2014, pp. 370–371.
- [6] X. Liu, S. Yao, S. V. Georgakopoulos, and M. M. Tentzeris, "Origami quadrifilar helix antenna in UHF band," in *Proc. Antennas Propag. Soc. Int. Symp. (APSURSI)*, Memphis, TN, USA, 2014, pp. 372–373.
- [7] S. Yao, X. Liu, S. V. Georgakopoulos, and M. M. Tentzeris, "A novel reconfigurable origami spring antenna," in *Proc. Antennas Propag. Soc. Int. Symp. (APSURSI)*, Memphis, TN, USA, 2014, pp. 374–375.
- [8] X. Liu, S. V. Georgakopoulos, and M. M. Tentzeris, "A novel mode and frequency reconfigurable origami quadrifilar helical antenna," in *Proc. Wireless Microw. Technol. Conf. (WAMICON)*, Cocoa Beach, FL, USA, 2015, pp. 1–3.
- [9] X. Liu, S. Yao, S. V. Georgakopoulos, B. S. Cook, and M. M. Tentzeris, "Reconfigurable helical antenna based on an origami structure for wireless communication system," in *Proc. IEEE MTT-S Int. Microw. Symp. (IMS)*, Tampa, FL, USA, 2014, pp. 1–4.
- [10] S. Yao, S. V. Georgakopoulos, B. S. Cook, and M. M. Tentzeris, "A novel reconfigurable origami accordion antenna," in *Proc. IEEE MTT-S Int. Microw. Symp. (IMS)*, Tampa, 2014, pp. 1–4.
- [11] L. J. Fei and D. Sujan, "Origami theory and its applications: A literature review," *World Acad. Sci. Eng. Technol.*, vol. 7, no. 1, pp. 113–117, 2013.
- [12] S. J. Mazlouman, A. Mahanfar, C. Menon, and R. G. Vaughan, "Reconfigurable axial-mode helical antenna," U.S. Patent 8436784 B2, May 7, 2013.
- [13] S. J. Mazlouman, A. Mahanfar, C. Menon, and R. G. Vaughan, "Reconfigurable axial-mode helix antennas using shape memory alloys," *IEEE Trans. Antennas Propag.*, vol. 59, no. 4, pp. 1070–1077, Apr. 2011.

- [14] C. A. Balanis, "Travelling wave and broadband antennas," in *Antenna Theory Analysis and Design*, 3rd ed. Hoboken, NJ, USA: Wiley, 2005, ch. 10, pp. 566–572.
- [15] A. R. Djordjević, A. G. Zajić, M. M. Ilić, and G. L. Stüber, "Optimization of helical antennas," *IEEE Antennas Propag. Mag.*, vol. 48, no. 6, pp. 107–116, Dec. 2006.
- [16] T. Nojima, "Modelling of folding patterns in flat membranes and cylinders by origami," *JSME Int. J. Ser. C*, vol. 45, no. 1, pp. 364–370, 2002.
- [17] L. Yang, A. Rida, R. Vyas, and M. M. Tentzeris, "IEEE RFID tag and RF structures on a paper substrate using inkjet-printing technology," *IEEE Trans. Microw. Theory Techn.*, vol. 55, no. 12, pp. 2894–2901, Dec. 2007.
- [18] K. Shinyama, T. Oi, and S. Fujita, "Dielectric relaxation phenomena of polylactic acid with  $\beta$ -crystalline chitin," *Int. J. Polym. Sci.*, vol. 2012, pp. 1–5, 2012.

## High-Sensitivity Ground Radiation Antenna System Using an Adjacent Slot for Bluetooth Headsets

Longyue Qu, Rui Zhang, and Hyeongdong Kim

**Abstract**—In this communication, we introduce a high-sensitivity antenna system for Bluetooth headsets dealing with the numerous and unidentified noises in a printed circuit board (PCB). This antenna system is composed of a ground radiation antenna for Bluetooth applications and an adjacent slot for noise suppression. A loop-type circuit is used to model a noise source on the PCB to provide wide-frequency spectrum noise currents to analyze the noise performance of the high-sensitivity antenna system. Decoupling between the noise sources and the antenna port can lead to high sensitivity. An adjacent slot is designed as part of the system to improve the sensitivity, based on the decoupling theorem. This proposed system is effective and applicable for high-sensitivity antenna design, as verified through simulation and active measurements of Bluetooth headsets.

**Index Terms**—Decoupling, ground radiation antenna, high-sensitivity antenna system, noise suppression.

### I. INTRODUCTION

In wireless communication systems where good performance on indexes such as signal-to-noise ratio (SNR) and bit error rate (BER) is highly demanded, noise performance has an important impact on antenna receiving properties, especially in RF systems. The effect of noise is critical because the noise power determines the minimum signal level that can be reliably recognized by the receiving antenna [1]. For a wireless system, the noise sources are composed of intrinsic noises caused by random process in an RF receiving chip, and

Manuscript received January 29, 2015; revised July 28, 2015; accepted September 08, 2015. Date of publication September 24, 2015; date of current version November 25, 2015. This work was supported by the ICT R&D program of MSIP/IITP, South Korea (B0101-15-1271, Ground radiation technique for mobile devices).

The authors are with the Department of Electronics and Computer Engineering, Hanyang University, Seoul 04763, South Korea (e-mail: hdkim@hanyang.ac.kr).

Color versions of one or more of the figures in this communication are available online at <http://ieeexplore.ieee.org>.

Digital Object Identifier 10.1109/TAP.2015.2481919

man-made noises coexisting in the PCB, such as digital and switching signals. In antenna design stage, the former is predetermined and fundamentally determines the intrinsic sensitivity of the receiver, which is the minimal power that can be detected by the RF chip, whereas the latter is a serious problem for antenna design that greatly degrades antenna sensitivity. The noise currents from the latter noise sources are introduced from the ground plane, which will interfere with the antenna circuit and introduce undesired signals, affecting the sensitivity of the receiving antenna. Usually, a careful PCB design is required for noise mitigation, which can be definitely of great help for antenna sensitivity and has been deeply studied in [2] and [3]. In active measurements, total isotropic sensitivity (TIS), which is strongly related to the antenna efficiency, conductive sensitivity, and noise interference, is a key parameter to evaluate the noise performance of a receiving antenna [4]. Thus, a receiving antenna can have better sensitivity by improving the antenna efficiency and/or reducing the interfering noise power. Accordingly, the antenna-related techniques, which are demonstrated in this communication, can be a supplementary practice to noise reduction problems.

There are some studies in [5]–[7], using a parasitic slot for decoupling in MIMO system where decoupled objects are identifiable and aggressive antennas. However, it has not been widely discussed how to deal with the numerous, unidentifiable, and randomly distributed noise problems where a tunable and controllable design is also necessary in practical applications. In this communication, we present a high-sensitivity Bluetooth antenna system, including a ground radiation antenna which is a small loop-type antenna that employs the ground plane as a dipole-type radiator [8]–[10], and a capacitor-loaded adjacent slot which can suppress the received noise power without affecting the characteristics of the antenna. Also, a noise source circuit is modeled to study the noise performance of the antenna system, which can be extended to the case where numerous noise sources are present in the PCB. The adjacent slot introduces different noise performance, and it can effectively be used to suppress noise sources in the Bluetooth operating band, which is the most important property in the proposed high-sensitivity antenna system. We further discuss the adjacent slot on the design principles and operation mechanisms, including the capacitor value, slot size, and location relative to the antenna. The proposed antenna system is analyzed by simulation, and the antenna property and noise performance are verified by active measurements of Bluetooth headsets in a  $6\text{ m} \times 3\text{ m} \times 3\text{ m}$  three-dimensional (3-D) CTIA OTA chamber by a TC-3000B Bluetooth tester.

### II. HIGH-SENSITIVITY ANTENNA SYSTEM DESIGN

As shown in Fig. 1, the proposed high-sensitivity antenna system is designed on a simplified PCB ground plane of a Bluetooth headset that is printed on a low-cost FR4 substrate with a thickness of 1 mm and dielectric constant  $\epsilon_r = 4.4$ . The ground radiation antenna is composed of a  $5\text{ mm} \times 7\text{ mm}$  radiation loop terminated with a radiation capacitor  $C_R$  and a  $2.5\text{ mm} \times 4\text{ mm}$  feeding loop terminated with a feeding capacitor  $C_F$ . The input impedance and the resonant frequency can easily be controlled by adjusting  $C_F$  and  $C_R$ , respectively. The ground radiation antenna and an adjacent slot constitute the two basic components of the high-sensitivity antenna system, responsible for wireless communication and noise suppression, respectively. The width and length of the slot are  $1\text{ mm}$  and  $L = 5\text{ mm}$ , respectively, at an edge-to-edge distance  $D$  of  $2\text{ mm}$  from the antenna; the open end of the slot is terminated with a capacitor  $C_S$  for sensitivity optimization. In the operating frequency of Bluetooth services, the values of  $C_F$  and  $C_R$  are chosen to be  $0.45$  and  $0.25\text{ pF}$ , respectively. The value of  $C_S$  is